International Journal of Non-Linear Mechanics 144 (2022) 104083

Contents lists available at ScienceDirect

International Journal of Non-Linear Mechanics

journal homepage: www.elsevier.com/locate/nlm

A toy model of misfolded protein aggregation and neural damage propagation in neurodegenerative diseases

S. Sampaoli [a], A. Agosti [b], G. Pozzi [a], P. Ciarletta [a,*]

[a] MOX Laboratory, Department of Mathematics, Politecnico di Milano, Piazza Leonardo da Vinci 32, 20133 Milano, Italy
[b] Dipartimento di Matematica 'F. Casorati', Università degli Studi di Pavia, Via Ferrata 5, 27100 Pavia, Italy

ARTICLE INFO

Keywords:
Neurodegenerative disease
Diffuse interface model
Allen-Cahn equation
Cahn–Hilliard equation
Finite element method

ABSTRACT

Neurodegenerative diseases (NDs) result from the transformation and accumulation of misfolded proteins within the nervous system. Several mathematical models have been proposed to investigate the biological processes underlying NDs, focusing on the kinetics of polymerization and fragmentation at the microscale and on the spread of neural damage at a macroscopic level. The aim of this work is to bridge the gap between microscopic and macroscopic approaches proposing a toy partial differential model able to take into account both the short-time dynamics of the misfolded proteins aggregating in plaques and the long-term evolution of tissue damage. Using mixtures theory, we consider the brain as a biphasic material made of misfolded protein aggregates and of healthy tissue. The resulting Cahn–Hilliard type equation for the misfolded proteins contains a growth term depending on the local availability of precursor proteins, that follow a reaction–diffusion equation. The misfolded proteins also possess a chemotactic mass flux driven by gradients of neural damage, that is caused by local accumulation of misfolded protein and that evolves slowly according to an Allen-Cahn equation. The diffuse interface approach is new for NDs and allows both to consider five different time-scales, from phase separation to neural damage propagation, and to reduce the computational costs compared to existing multi-scale models, allowing a time-step adaptivity. We present here numerical simulations in a simple two-dimensional domain, considering both isotropic and anisotropic mobility coefficients of the misfolded protein and the diffusion of the neural damage, finding that the spreading front of the neural damage follows the direction of the largest eigenvalue of the mobility tensor. In both cases, we computed two biomarkers for quantifying the aggregation in plaques and the evolution of neural damage, that are in qualitative agreement with the characteristic Jack curves for many NDs.

1. Introduction

Neurodegenerative diseases (NDs) such as Alzheimer's disease (AD), Parkinson's disease and amyotrophic lateral sclerosis, result from the transformation and accumulation of specific proteins within the nervous system [1]. They result into a neuronal degeneration that could lead to cognitive impairment, dementia, motor difficulties, psychological and behavioural disorders. Typically NDs have common features, like the chronic and progressive nature, the destruction of neurons in specific areas of the brain, the damage of the synaptic connections network, and the increase of prevalence with age. Most importantly, they all display a common biochemical origin, that is the accumulation of misfolded protein aggregates [2].

There is experimental evidence that the proteins involved in NDs acquire their pathogenicity by a prion-like mechanism. Indeed, the pathogenic proteins are released by a cell in the extracellular fluid. They later move into other cells, where they act as seeds and induce misfolding of healthy protein [3]. The most important seed-proteins are amyloid-β (involved in senile plaques formation in AD), tau (involved in tauopathies) and α-synuclein (in Lewy-diseases). In physiological conditions the conformation of these proteins ensures the solubility and thus the correct secretion. In NDs the protein is misfolded, it shows an increase in the β-sheet structure getting into a pathologic aggregate-fibrillar state. The misfolded protein, at the beginning, gives small oligomers that increase in size till they form large aggregates. The aggregates of all sizes are toxic for cells, and thus for neurons, and they lead to neural damage [2]. On the other hand, the neural damage activates the amyloid precursor proteins involved in the cells signalling driven by synapse retraction, which in turn induce an increase in the amyloid-β production [4]. Thus, amyloid-β synaptotoxicity drives amyloid-β production in a positive feedback loop.

Several mathematical models have been proposed to investigate the biological processes underlying NDs at different scale. At a microscopic level, Smoluchowski equations are often used to describe

* Corresponding author.
E-mail address: pasquale.ciarletta@polimi.it (P. Ciarletta).

https://doi.org/10.1016/j.ijnonlinmec.2022.104083
Received 7 February 2022; Received in revised form 6 May 2022; Accepted 7 May 2022
Available online 20 May 2022

the self-association among monomers and polymers of different sizes for describing the elongation of fibrils by end-to-end formation [5–8]. Further models include the role of prions [9], the growth kinetics of amyloids [10–12], and the use of network-approaches to understanding the behaviour of different brain regions [13,14]. At the macroscopic level, the spreading of neural damages is typically modelled through a nonlinear reaction–diffusion mechanism [15,16], that can be effectively coupled with nucleation–aggregation–fragmentation models for the dynamics in the brain connectome [17,18]. Multiscale approaches have been proposed in [19,20], assuming that the damage diffuses in the neuronal net through a neuron-to-neuron prion-like propagation mechanism and that monomeric form of the amyloid spreads through the brain tissue undergoing agglomeration.

The aim of this work is to bridge the gap between microscopic and macroscopic approaches proposing a toy partial differential model able to take into account both the short-time dynamics of the misfolded proteins aggregating in plaques and the long-term evolution of neural damage. In particular, we are focused on modelling the evolution of the disease starting from a delimited brain region presenting an hoarding of amyloid-β and amyloid precursor proteins. The article is organized as follows. In Section 2, we introduce the mathematical model and in Section 3 we perform its dimensional analysis. In Section 4, we describe its numerical implementation and we discuss the numerical results in few test cases. We also propose two biomarkers to be compared with the ones used for describing the progressing of NDs. In Section 5 we collect few concluding remarks.

2. The mathematical model

We consider the brain tissue as a binary, saturated, closed and incompressible mixture composed by a protein phase of proliferating plaques and a healthy phase representing the host tissue. Let ϕ_p and ϕ_t be the volume fraction of the plaques and the healthy tissue, respectively. Assuming that both phases have the same mass density γ, the following continuity equations hold:

$$\begin{aligned} &\frac{\partial \phi_p}{\partial t} + \nabla \cdot (\phi_p \mathbf{v}_p) = \frac{S_p}{\gamma} + \nabla \cdot \mathbf{k}_p, \\ &\frac{\partial \phi_t}{\partial t} + \nabla \cdot (\phi_t \mathbf{v}_t) = \frac{S_t}{\gamma} + \nabla \cdot \mathbf{k}_t, \end{aligned} \tag{1}$$

where $\mathbf{v}_i$, with $i = (p, t)$, is the velocity of the ith phase, S_i is the volumetric source term and $\mathbf{k}_i$ is the non-convective mass flux. The mixture is saturated, i.e.

$$\phi_p + \phi_t = 1, \tag{2}$$

and it is not growing, i.e.

$$S_p + S_t = 0; \qquad \mathbf{k}_p + \mathbf{k}_t = \mathbf{0}. \tag{3}$$

in order to locally satisfy the conservation of mass exchanged between the phases. Accordingly, the continuity equation for the whole mixture obtained summing up the two equations in (1) reads:

$$\nabla \cdot (\phi_p \mathbf{v}_p + \phi_l \mathbf{v}_t) = 0. \tag{4}$$

Following [21,22], we use the principle of maximum dissipation to obtain the constitutive laws for phase velocities. In particular, we aim to find the stationary values of the Rayleghian $\mathfrak{R}$, defined as:

$$\mathfrak{R} = W + \frac{dE}{dt}, \tag{5}$$

where W is the energy dissipation and E is the Landau free energy of the system. We assume that the main dissipation source is given by the viscous interactions due to the relative motion between the phases, i.e.

$$W = \frac{1}{2} \int_\Omega \phi_p (\mathbf{v}_p - \mathbf{v}_t)^T \mathbf{M} (\mathbf{v}_p - \mathbf{v}_t) dV, \tag{6}$$

where $\mathbf{M} = M_0 \mathbf{T}^{-1}$, is a tensor representing volumetric friction, that is inversely proportional to the preferential directions tensor $\mathbf{T}$, M_0 is a friction parameter, and Ω represents the whole brain. The tensor $\mathbf{T}$ takes into account the local anisotropy of the brain micro-structure, and it can be extracted from clinical neuroimaging data, such as diffusion tensor imaging.

The Landau free energy E reads:

$$E = \int_\Omega \left(\frac{\gamma_\phi^2}{2} |\nabla \phi_p|^2 + \Psi(\phi_p) \right) dV, \tag{7}$$

where $\Psi(\phi_p)$ is a local interaction potential of the Lennard-Jones type, while the quadratic gradient terms is a short-range nonlocal potential governed by the small parameter γ_ϕ. In particular, we assume that the interaction force given by $\Psi'(\phi_p)$ has the following form:

$$\Psi'(\phi_p) = F \frac{\phi_p^2 (\phi_p - \phi_e)}{1 - \phi_p},$$

where F is a characteristic interaction energy density. The previous equation represents a phenomenological law introduced in [23], in which the plaques behave as an elastic fluid subjected to repulsion at high volume density of plaques, to attraction at low density and to homeostasis for an equilibrium value ϕ_e. Since $\Psi(\phi_p)$ is non-convex, the gradient term in (7) acts as a regularizing effect that creates a diffuse interface between region with higher and lower concentration of plaques. Assuming that the mixture is highly viscous and that the tissue behaves as a perfect fluid [24], following [25] we derive a Cahn–Hilliard type equation for the plaque concentration:

$$\begin{cases} \dfrac{\partial \phi_p}{\partial t} = \nabla \cdot \left(\dfrac{\phi_p (1 - \phi_p)^2}{M_0} \mathbf{T} \nabla \mu \right) + \dfrac{S_p}{\gamma} + \nabla \cdot \mathbf{k}_p, \\ \mu = \Psi'(\phi_p) - \gamma_\phi^2 \Delta \phi, \end{cases} \tag{8}$$

where we have to define the constitutive equations for the non-convective mass flux $\mathbf{k}_p$ and the source term S_p from a biological viewpoint. In particular, following [19], we hypothesize that the damage diffuses in the neuronal net through a neuron-to-neuron prion-like propagation mechanism and that monomeric form of the protein spreads through the microscopic tortuousness of the brain tissue undergoing agglomeration. Eventually this leads to the formation of long, insoluble fibrils, accumulating in spherical deposits known as senile plaques that become toxic for neurons, creating a spreading brain damage. Therefore, we introduce a variable n defining the neuronal damage in the brain, and we assume that the non-convective mass flux is due to chemotactic motion of plaques with respect to the gradient of the neuronal damage, such as:

$$\mathbf{k}_p = k_n \phi_p \mathbf{T} \nabla n, \tag{9}$$

where k_n is the chemotactic coefficient. Here, we base on the experimental evidence that misfolded proteins migrate towards regions characterized by lower neural damage and react with non-misfolded proteins [26].

Similarly, we assume that the volumetric source of plaques is proportional to the local concentration p of precursor proteins, such as amyloid precursor proteins, such that:

$$S_p = \nu_p \gamma \phi_p \left(\frac{p}{p_s} - \delta \right) (1 - \phi_p), \tag{10}$$

where ν_p is the plaque proliferation rate, p_s is the physiological concentration of precursor proteins in the brain tissue and δ is a threshold value, which sets the lower value over which there is an over accumulation of precursor proteins. The growth of plaques follows a logistic law, with saturation when the plaques occupy all the available volume for $\phi_p = 1$.

We assume that the precursor proteins undergo a reaction–diffusion dynamics, being:

$$\frac{\partial p}{\partial t} = D_p \nabla \cdot (\mathbf{T} \nabla p) + S_n ((1 - n) \chi_C + n)(p_s - p) - \delta_p \phi_p p. \tag{11}$$

A reaction diffusion dynamics is justified by the experimental observation that large extra-cellular vesicles, that are vehicles for the precursor

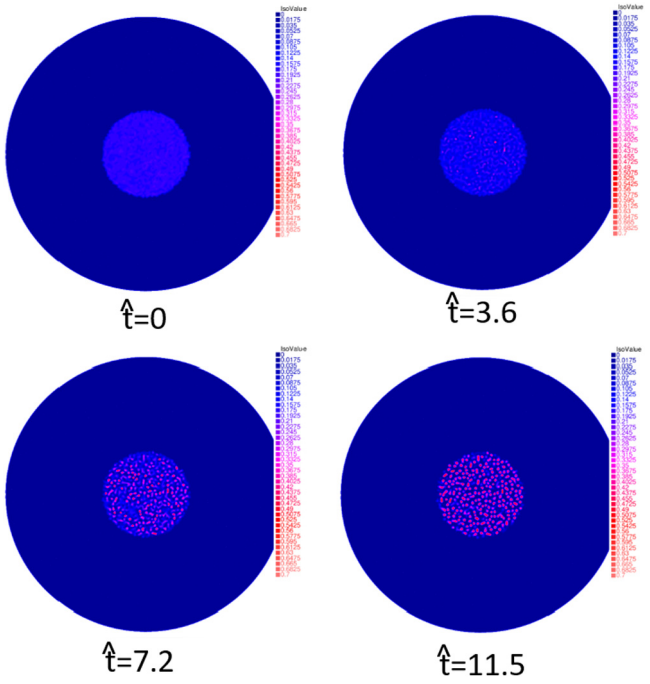

Fig. 1. Colourmap of the spatial distribution of ϕ_p during the early stage dynamics, shown at $\hat{t} = 0, 3.6, 7.2, 11.5$ setting $\hat{k} = 2.5$, $\hat{D}_n = 1$. We observe the initial phase separation into circular aggregates of plaques and the subsequent coarsening dynamics of the clusters.

proteins, exploits the prion protein and its binding-unbinding kinetics on its neuronal receptors to actively move on the neuron surface, across the synapse and to reach distant target regions [27]. Here, we are assuming that there is a region Ω_C in which initially there is a hoarding of precursor proteins and where the plaques formation begins even in the absence of neural damage, with χ_C its indicator function. Outside of Ω_C, damage propagation triggers the accumulation of precursor proteins, which enhances the formation of plaques, thus modelling the pathogenic positive feedback loop between amyloid production and synapse damage reported in literature [4]. Hence, the source term $S_n\beta((1-n)\chi_C + n)(p_s - p)$ describes the growth rate of precursor proteins in Ω_C and in regions where the neural damage propagates, and δ_p is the consumption rate of proteins by the plaques.

Moreover, assuming that n propagates following the same pathway of the electrical signal in the brain, we describe the neural damage dynamics as follows:

$$\frac{\partial n}{\partial t} = \epsilon D_n \nabla \cdot (\mathbf{D}\nabla n) - \epsilon K_n n(n-1)(n-\alpha) + \epsilon C_s \chi_{C_n}(K(\phi_p) - \delta_n)(1-n). \tag{12}$$

Indeed, Eq. (12) is an Allen-Cahn bistable equation, often adopted to model the signal propagation in presence of damage [28]. Here, the neural damage is taken into account by the term $\epsilon C_s \chi_{C_n}(K(\phi_p) - \delta_n)(1-n)$, where $K(\phi_p)$ is the fractional area occupied by the plaques in Ω_C and defined as $K(\phi_p) = \frac{\int_{\Omega_C} I_{(\phi_p > 0.3)}}{\int_{\Omega_C} d\Omega}$, where $\int_{\Omega_C} I_{(\phi_p > 0.3)}$ is the volume in which ϕ_p is bigger than the threshold value 0.3. Moreover, χ_{C_n} represents a Gaussian function supported over the circular damaged area in order to represent the damage onset in the centre, δ_n is the threshold above which the plaques create neuronal damage and C_s is the neural damage proliferation rate. Moreover, we include a small dimensionless parameter ϵ accounting for the fact that the spreading dynamics of the neural damage is much slower than the dynamics of protein misfolding and agglomeration. On the other hand, the two-dimensional propagation is described from the first two terms at the right hand side of Eq. (12), where D_n is a diffusion coefficient, $\mathbf{D}$ is the tensor of the preferential directions of the expansion of damage and K_n is a sink proliferation rate. We further remark that the term α is required to belong to the range $(0, \frac{1}{2})$ in order to allow the existence of a travelling wave solution.

3. Dimensional analysis

The partial differential model is made by Eqs. (8), (11), (12) equipped with no-flux conditions for the variables ϕ_p, μ, n, p on the brain boundary. We first remark that the partial differential system has multiple time-scales, namely:

- the phase separation and coarsening of ϕ_p, i.e. $t_1 \sim \epsilon \frac{M_0 \gamma_\phi^2}{F^2}$;
- the proliferation rate of ϕ_p, i.e. $t_2 \sim \frac{\epsilon}{\nu_p}$;
- the interaction between the precursor protein and the plaques, i.e. $t_3 \sim \frac{M_0 D_p}{F \delta_p}$
- the diffusion of n, i.e. $t_4 \sim \frac{F}{\epsilon M_0 \nu_p D_n}$;
- the proliferation rate of the neuronal damage, i.e. $t_5 \sim \frac{1}{\epsilon C_S}$.

For the sake of simplicity, let us first introduce the following dimensionless variables:

$$\hat{p} = \frac{p}{p_s}, \qquad \hat{n} = n, \qquad \hat{\mu} = \frac{\mu}{F}, \qquad \hat{t} = t\nu_p, \qquad \hat{x} = x\sqrt{\frac{\delta_p}{D_p}}.$$

After standard manipulations we obtain the following dimensionless system:

$$\begin{cases} \dfrac{\partial \phi_p}{\partial \hat{t}} = \hat{D}\hat{\nabla} \cdot \left(\phi_p(1-\phi_p)^2 \mathbf{T}\hat{\nabla}\hat{\mu} \right) + \phi_p(\hat{p} - \delta)(1-\phi_p) + \hat{k}\hat{\nabla} \cdot (\phi_p \mathbf{T}\hat{\nabla}\hat{n}), \\ \hat{\mu} = \hat{f} - \hat{\gamma}_\phi \hat{\Delta}\phi_p, \\ \dfrac{\partial \hat{p}}{\partial \hat{t}} = \hat{v}\left(\hat{\nabla} \cdot (\mathbf{T}\hat{\nabla}\hat{p}) + \hat{\beta}((1-\hat{n})\chi_C + \hat{n})(1-\hat{p}) - \phi_p \hat{p} \right), \\ \dfrac{\partial \hat{n}}{\partial \hat{t}} = \epsilon \hat{D}_n \hat{\nabla} \cdot (\mathbf{D}\hat{\nabla}\hat{n}) - \epsilon \hat{K}_n \hat{n}(\hat{n}-1)(\hat{n}-\alpha) + \epsilon \hat{C}_s \chi_{C_n}(K(\phi_p) - \delta_n)(1-\hat{n}), \end{cases} \tag{13}$$

that is governed by the following dimensionless parameters:

$$\hat{D} = \frac{F\delta_p}{\nu_p D_p M_0}, \quad \hat{k} = \frac{\delta_p k_n}{D_p \nu_p}, \quad \hat{\gamma}_\phi = \frac{\gamma_\phi^2 \delta_p}{D_p F}, \quad \hat{v} = \frac{\delta_p}{\nu_p},$$
$$\hat{f} = \frac{1}{F}\frac{\partial \Psi_\phi}{\partial \phi}, \quad \beta = \frac{S_p}{\delta_p}, \quad \hat{D}_n = \frac{D_n \delta_p}{\nu_p D_p}, \quad \hat{K}_n = \frac{K_n}{\nu_p}, \quad \hat{C}_s = \frac{C_s}{\nu_p}, \quad \epsilon.$$

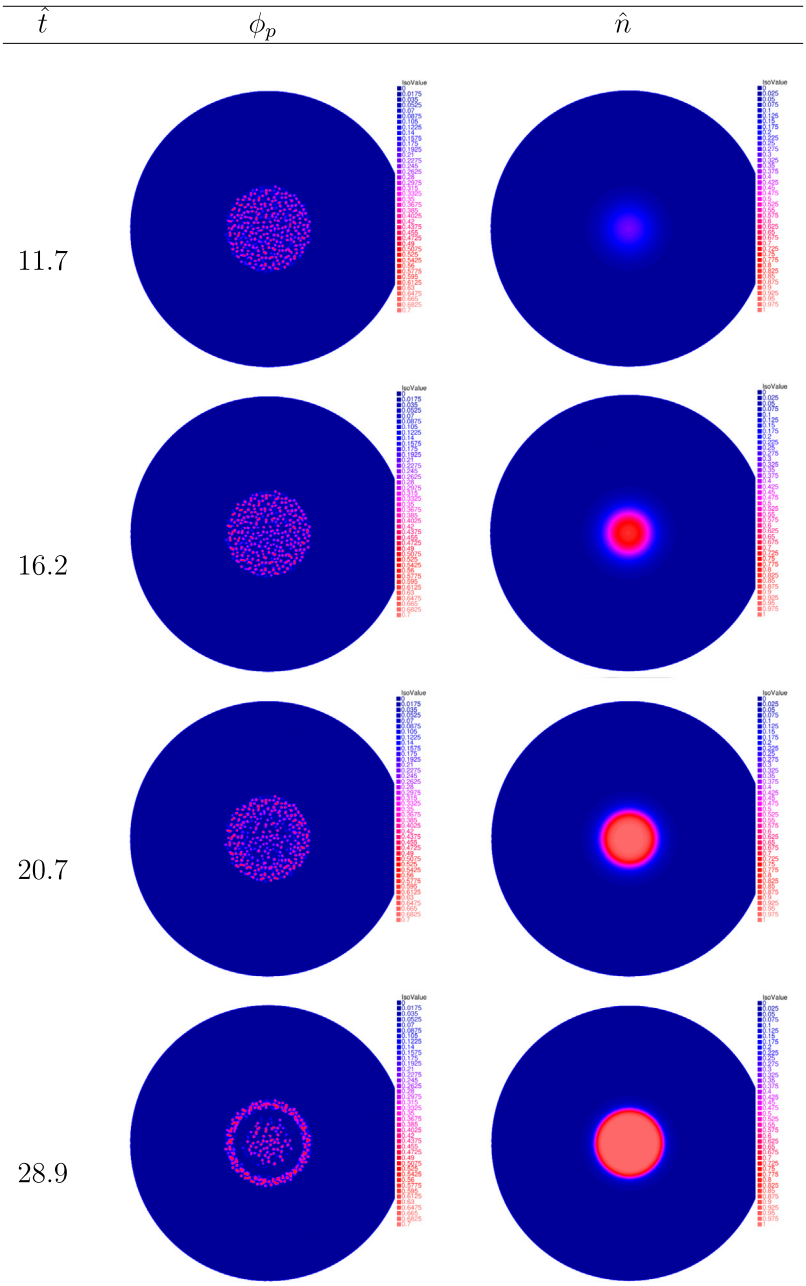

Fig. 2. Colourmap of the spatial distribution of ϕ_p and $\hat{n}$ during the later stages of dynamics, shown at $\hat{t} = 11.7, 16.2, 20.7, 28.9$ setting $\hat{k} = 2.5$, $\hat{D}_n = 1$ for the isotropic case. We observe the plaques spreading (left) and the onset of the neural damage after plaques clustering (right).

4. Numerical results

4.1. Finite element implementation

The dimensionless model in (13) is numerically solved using the library FreeFEM++ for solving partial differential equations using finite element method [29]. The finite element approximation of the model preserves the physical bounds for the variables representing plaques and the neural damage, that are non-negative and smaller or equal to one. Moreover, the introduction of the degenerate mobility in the Cahn–Hilliard equation makes the solution not unique. In the numerical formulation we go beyond the latter issue introducing a subdivision of the nodes of the mesh domain into active and passive nodes, following [30,31]. The lumping approximation of the mass scalar products in the finite element discretization is introduced in order for the discrete solution to be able to track compactly supported solutions of Cahn–Hilliard equation with a free boundary which moves with a finite speed. This method allows to select the physical solutions with compact support and moving boundary. Moreover we have taken into account both the dissipative behaviour of the system, that is not preserved at the discrete level, by introducing a splitting of the energy functional into a convex and a concave part, and the positivity of the ϕ_p by imposing a variational inequality following the algorithm proposed in [32]. The associated gradient projection algorithm is formulated in terms of a backtracking line search method, in order to optimize the choice of the descent coefficient, using the Armijo method [33], based on the Armijo–Goldstein condition as in algorithm proposed by [34]. Moreover we developed a time step adaptivity procedure for taking into account all the time scales of the system dynamics, from the phase separation of the plaques to the spread of neural damage.

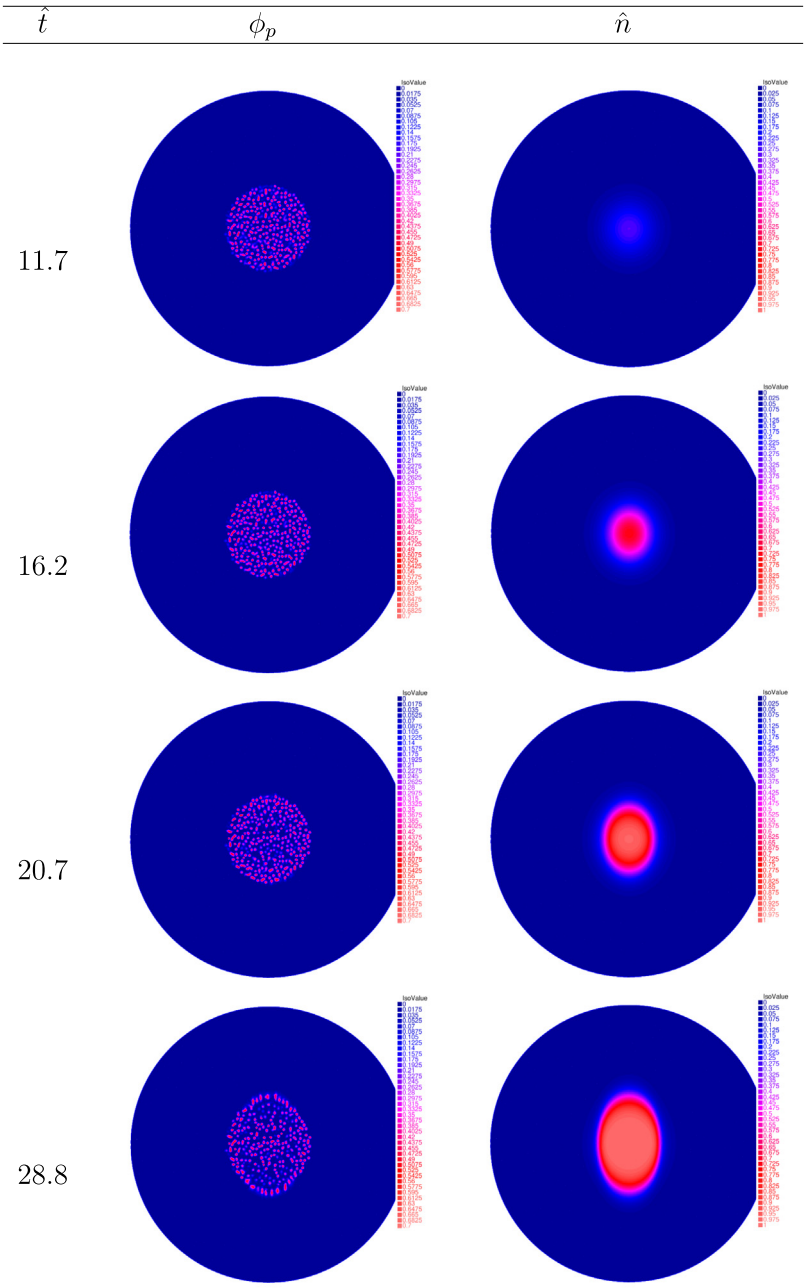

Fig. 3. Colourmap of the spatial distribution of ϕ_p and $\hat{n}$ during the later stages of dynamics, shown at $\hat{t} = 11.7, 16.2, 20.7, 28.9$ setting $\hat{k} = 2.5$, $\hat{D}_n = 1$ for the anisotropic case. We observe that both the neural damage and the plaque distribution follows the preferential direction of the mobility tensor $\mathbf{T}$ showing an elliptic shape.

Finally, we performed numerical simulations on a two dimensional circular domain centred in the origin with a dimensionless diameter equal to 100. Since we set the characteristic length to $\sqrt{(D_n/\delta_n)} = 0.1$ mm, it corresponds to a physical domain whose diameter is of 1 cm. We subdivided the domain in triangles, choosing 124 elements for each side in order to evaluate the plaques formation and the neural damage propagation and we used continuous linear elements. Since this is the first attempt to define a diffuse interface model for NDs and we are interested in the qualitative analysis of its solution, we use in the following the biological range for the model parameters taken from previous works on brain tumours [35,36]. In particular, we fix the values of the dimensionless parameters as $\epsilon = 0.1$, $\hat{D} = 4.48$, $\hat{\gamma}_\phi = 0.03$, $\hat{v} = 1000$, $\hat{\beta} = 0.045$, $\hat{K}_n = 10\epsilon$, $\hat{C}_s = 5.5$, $\beta = 0.045$, $\alpha = 0.2$, $\delta = \delta_n = 0.3$, $\phi_e = 0.6$, while we vary the values of $\hat{D}_n$ and $\hat{k}$ in the following test cases. The time step is set to $\Delta t = 0.5\ \hat{\gamma}_\phi^2$ for the first iteration and then it is determined step by step through the adaptive procedure. We choose the initial conditions $n(\mathbf{x},0) = n_0(\mathbf{x}) = 0$, $p(\mathbf{x},0) = p_0(\mathbf{x}) = \chi_C$ and $\phi_p(\mathbf{x},0) = \phi_0(\mathbf{x}) = (0.18 + 0.018 \cdot (1 - 2r))\chi_C$, where r is a random number sampled from the uniform distribution over $[0,1]$ and χ_C is the indicator function of the subdomain Ω_C, a circle centred at the middle of the domain with a dimensionless diameter equal to 25. The choice of the initial expression of $\phi_p(\mathbf{x},0)$ ensures that the initial density is in the metastable regime of the Cahn–Hilliard equation, thus the presence of a white noise is sufficient to trigger phase separation and coarsening.

4.2. Numerical simulations

We performed numerical simulations varying the dimensionless parameters $\hat{k}$, $\hat{D}_n$ in order to investigate the effects on the dynamics of the chemotaxis and of the diffusion of the neural damage, respectively. We also simulated two different cases of material microstructure, in

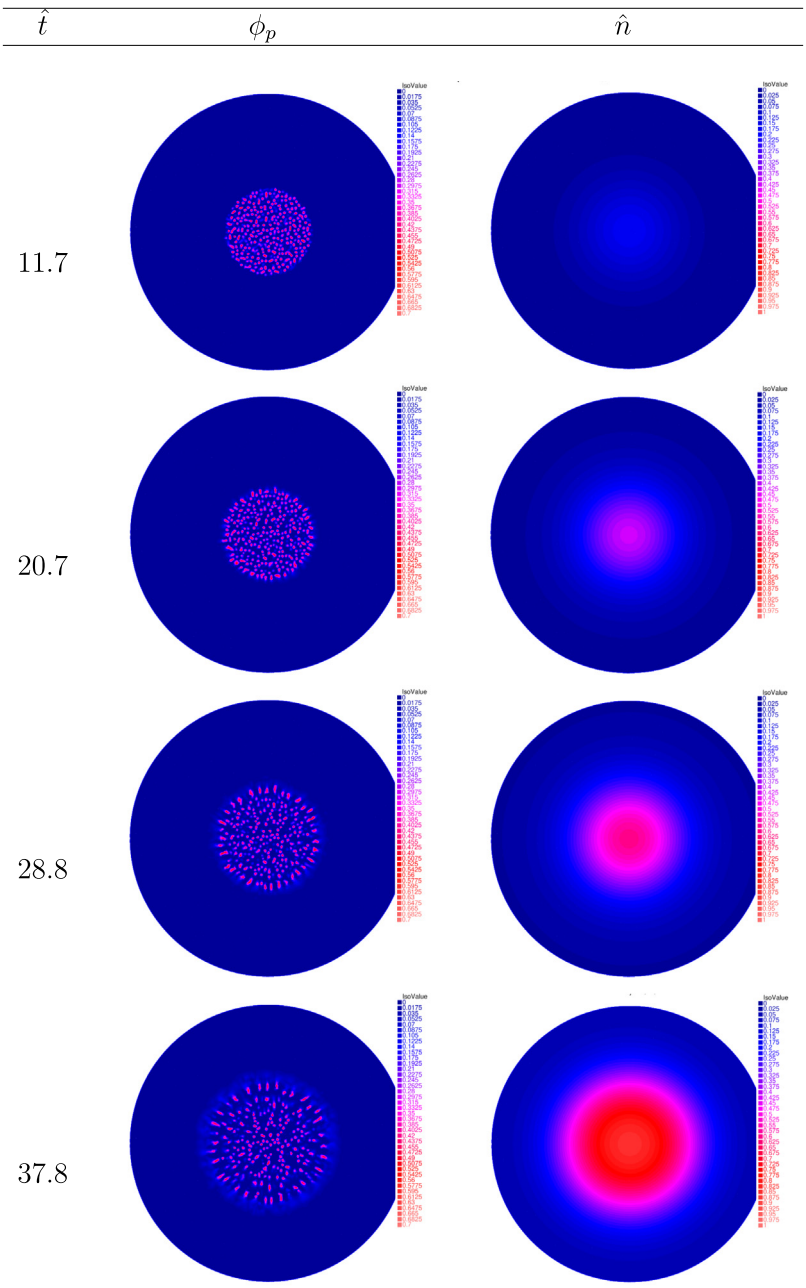

Fig. 4. Colourmap of the spatial distribution of ϕ_p and $\hat{n}$ during the later stages of dynamics, shown at $\hat{t} = 11.7, 20.7, 28.8, 37.8$ setting $\hat{k} = 25$, $\hat{D}_n = 10$ for the isotropic case.

which we give the following Cartesian expressions of the tensors **T** and **D**:

- isotropic case, i.e. $\mathbf{T} = \mathbf{D} = \text{diag}(1,\ 1)$;
- anisotropic case, i.e $\mathbf{D} = \text{diag}(1,\ 20)$ and $\mathbf{T} = \text{diag}(0.1,\ 1.9)$.

We performed the first set of simulations by imposing $\hat{k} = 2.5$, $\hat{D}_n = 1$, exploring both the isotropic and anisotropic scenarios. The early stage dynamics is about the same for both the two cases. As depicted in Fig. 1, we first observe the phase separation of the solution for ϕ_p, followed by a clustering dynamics without any formation of neuronal damage. We observe no significant qualitative difference between the isotropic and the anisotropic case.

The later stage dynamics for the isotropic case is depicted in Fig. 2. Once the plaque clusters are completely formed, the neural damage begins to expand. The plaques later spread through the healthy tissue following the radial direction of the damage growth, while the inner region becomes completely damaged.

Fig. 3 displays the numerical results for the anisotropic case, simulated with the same parameters values of the previous isotropic case, i.e. $\hat{k}_n = 2.5$, $\hat{D}_n = 1$. In this latter case, the neural damage starts growing at about $\hat{t} = 11.7$ and it immediately follows the preferential direction of the mobility tensor **T**, followed by the plaques. At the final step, we observe that both the damaged area and the plaque domain take an elliptic shape, highlighting the pivotal importance of the microstructure on the invasion dynamics.

We finally performed another set of simulations for both the isotropic and anisotropic cases. In this case, we increased of an order of magnitude the values of both the chemotactic and the damage diffusion parameters, thus setting $\hat{k} = 25$, $\hat{D}_n = 10$. We remark that increasing $\hat{D}_n = 10$ by an order of magnitude corresponds to make the diffusion time-scale t_4 one order of magnitude faster than the proliferation

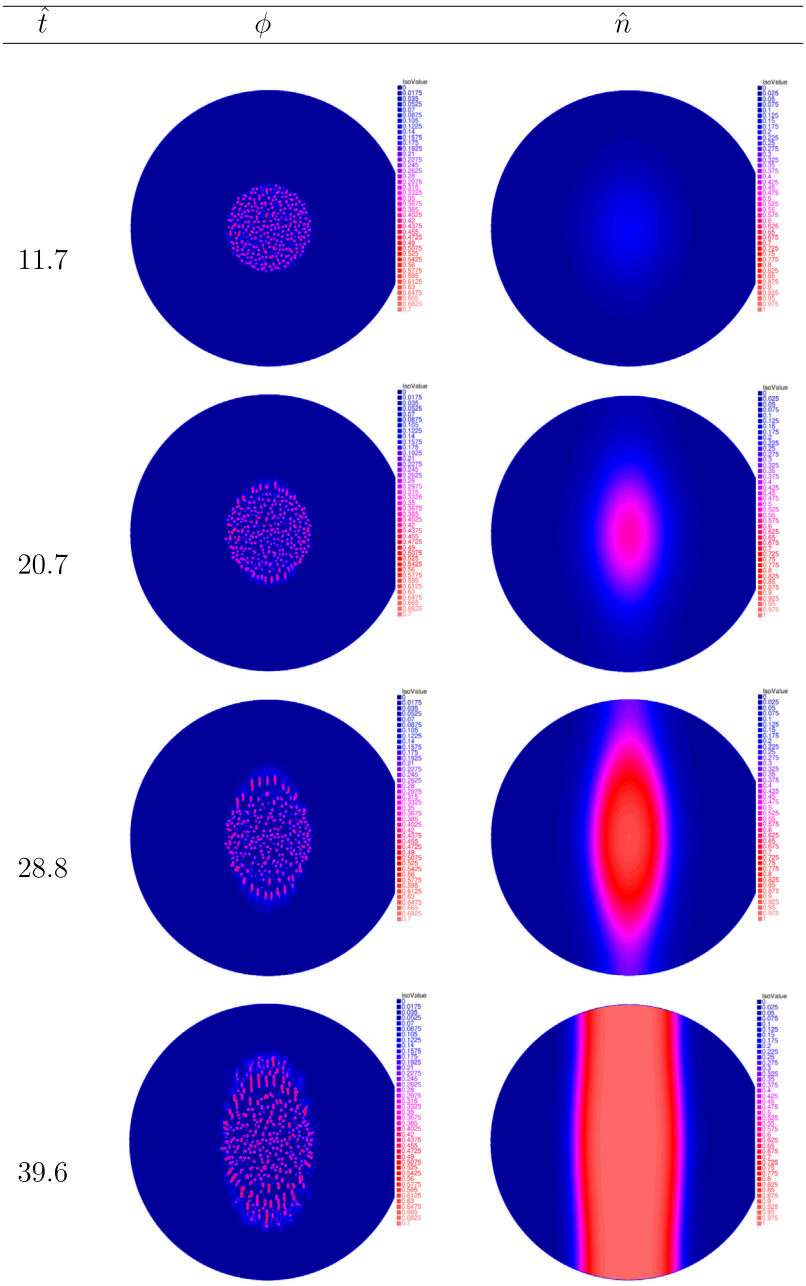

Fig. 5. Colourmap of the spatial distribution of ϕ_ρ and $\hat{n}$ during the later stages of dynamics, shown at $\hat{t} = 11.7, 20.7, 28.8, 37.8$ setting $\hat{k} = 25$, $\hat{D}_n = 10$ for the anisotropic case.

time-scale t_2, whilst the phase separation and coarsening time-scale are unaffected. In fact, we find that the initial stage dynamics is qualitatively the same observed in the previous cases, since $\hat{n}$ has a slow dynamics and its onset is completely determined by the phase separation dynamics of the Cahn–Hilliard equation without the chemotaxis term. A considerable difference from the previous scenarios can be appreciated from the simulation results collected in Figs. 4 and 5, for the isotropic and anisotropic cases respectively. In particular, as remarked earlier the increased $\hat{D}_n$ makes the neural damage propagating faster, and the increased $\hat{k}$ makes the plaques following faster the front of the neural damage wave.

4.3. Biomarkers

In order to provide a biological interpretation of our numerical results, we present here two biomarkers suitable for quantifying the accumulation of plaques and the extent of neurodegeneration, to be compared to the well known Jack curves [37].

In a clinical setting, a first biomarker is sought to investigate the plaque accumulation. For the Alzheimer Disease, such indicator can be identified with the CSF-Aβ_{42} and the amyloid PET. On the other hand, a second biomarker is used to describe the neurodegeneration since plaques can grow logistically reaching the saturation even decades before the patient experiences the first symptoms and before MRI or PET detect neuronal damage. Concerning this latter indicator, FDG-PET has been proven to be a promising modality for detecting functional brain changes in AD [38]. The evolution curves of both biomarkers are characterized by a sigmoidal shape with a large time shift.

Accordingly, here we propose two biomarkers for evaluation the simulated dynamics. Firstly, we define the average neural damage as:

$$B_n = \frac{\int_\Omega \hat{n}(x,t)dx}{\int_\Omega dx}, \tag{14}$$

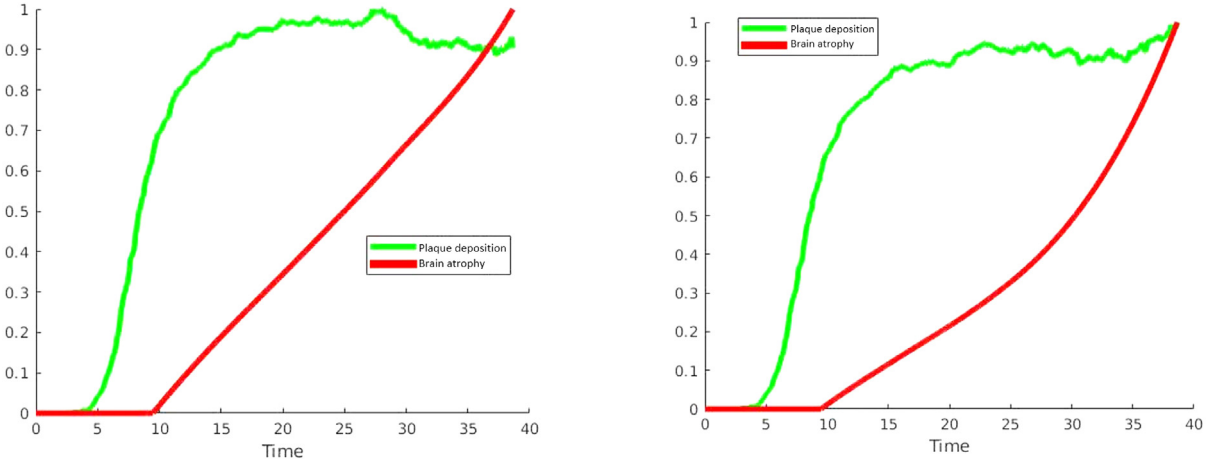

Fig. 6. Evolution of the normalized biomarkers B_p (green) and B_n (red) over the dimensional time expressed in years for both the isotropic (left) and anisotropic (right) case, setting $\hat{k} = 2.5$, $\hat{D}_n = 1$. (For interpretation of the references to colour in this figure legend, the reader is referred to the web version of this article.)

that is a measure of brain atrophy. Secondly, we define the average concentration of plaques over the whole computational domain as:

$$B_p = \frac{\int_\Omega I_{\phi_p > 0.3} dx}{\int_\Omega dx}, \tag{15}$$

where $I_{\phi_p > 0.3}$ is the indicator function introduced in Section 2.

In Fig. 6, we report the evolution of the two biomarkers B_n and B_p, normalized with respect to their maximum value, over the dimensional time t expressed in units of years. We observe that for both the isotropic and the anisotropic case, B_p grows earlier and faster than B_n, presenting the characteristic sigmoidal trend.

On the other hand, B_n starts growing over time as soon as B_p saturates, thus presenting a delay over time with respect to plaques deposition. Accordingly, B_n displays the typical short-time behaviour of the Jack curves for neural damage, that are also known to grow more slowly as disease progressed. Finally, we remark that the curves for B_n do not appear as sigmoidal as one should expect from Eq. (12). This discrepancy is due to the fact that we computed B_n over a time interval shorter than the characteristic time of the later development of brain atrophy, only to avoid excessive computational costs.

5. Conclusion

In this work we developed a toy model for describing both the short-time dynamics of misfolded protein aggregation in plaques and the long-term evolution of neural damage.

Using the theoretical framework of mixtures theory, we considered the brain as a biphasic material made of misfolded protein aggregates, interacting with a local Lennard-Jones potential and a nonlocal short-range term, and of healthy tissue behaving as a perfect fluid. The resulting Cahn–Hilliard type equation for the misfolded proteins contains a growth term depending on the local availability of precursor proteins, that follow a reaction–diffusion equation. The misfolded proteins also posses a chemotactic mass flux driven by gradients of neural damage, that is caused by local accumulation of misfolded protein and that evolves slowly according to an Allen-Cahn equation.

The partial differential model made by Eqs. (8), (11), (12) has been solved numerically using the finite element method in a simple two-dimensional domain, evaluating the effects of the mobility of the misfolded protein and the diffusion of the neural damage. We considered both isotropic and anisotropic mobility coefficients, highlighting that the spreading front of the neural damage follows the direction of the largest eigenvalue of the mobility tensor. In both cases, we computed two biomarkers to quantify the aggregation in plaques and the evolution of neural damage, that are in qualitative agreement with the characteristic Jack curves for many NDs.

This is the first attempt to use a diffuse interface approach to model both the fast fragmentation and segmentation dynamics at the microscale and the slow spreading of the neural damage at the tissue level. While existing multi-scale approach focus on the two-characteristic time scales of fragmentation and evolution of the disease proposing phenomenological laws to explain the slow transport of the newly formed, spatially localized aggregates [39], here the multi-scale spatial dynamics is dictated by underlying biological processes that evolve at five different time scales, determining the phase separation, the coarsening evolution, the propagation of the neural damage along preferential directions and the interaction between plaques and precursor proteins. In particular, the proposed Cahn–Hilliard equation for the plaques allows to bridge fast phase separation and clustering with a slow damage-driven coarsening phenomenon. This modelling choice allows to reduce significantly the numerical cost of solving the highly nonlinear microscopic kinetics equations for the misfolding at the microscale, without domain simplification as in [18], and to implement an adaptive time scale that allows to perform numerical simulation in a macroscopic domain for large time spans, thus avoiding the severe time-step constraints, such as the ones imposed by coupling parabolic and hyperbolic equations in [19].

The proposed toy model is a preliminary attempt to build a bridge between microscopic and macroscopic descriptions of NDs that is based on a first principles description of both the short- and long-time dynamics. As such, it suffers several limitations, as the lack of either a realistic polymerization kinetics of the misfolded proteins and of their neuron-to-neuron prion-like propagation mechanism, or the qualitative description of the presented numerical simulation in a simplified two-dimensional domain. These aspects must be addressed in the future in order to make the model relevant for the biological research community, e.g. building three-dimensional computational frameworks from neuroimaging data and accounting for more realistic constitutive equations for the different brain tissues, including the role of the glymphatic pathway for neurodegeneration, and allowing for much larger simulation times. Once these improvements will be achieved, the simulation results may guide the identification of undiscovered spreading pathways of the neural damage depending on the specific brain architecture of each patient, that can be reconstructed from diffusion tensor imaging into the tensors of diffusion and mobility of the proposed model, possibly being used as a predictive tool helping the clinician in the early screening of the pathology.

CRediT authorship contribution statement

S. Sampaoli: Formal analysis, Software, Review & editing. **A. Agosti:** Conceptualization, Supervision, Methodology, Formal analysis,

Software, Review & editing. **G. Pozzi:** Formal analysis, Review & editing. **P. Ciarletta:** Conceptualization, Supervision, Methodology, Formal Analysis, Review & editing.

Declaration of competing interest

The authors declare that they have no known competing financial interests or personal relationships that could have appeared to influence the work reported in this paper.

Acknowledgements

This work was supported by MUR PRIN 2017 grant 2017KL4EF3, by Regione Lombardia project NEWMED (Grant No. POR FESR 2014–2020) and partly by GNFM – INdAM through the program *Progetto Giovani 2020*.

References

[1] M. Jucker, L.C. Walker, Self-propagation of pathogenic protein aggregates in neurodegenerative diseases, Nature 501 (7465) (2013) 45–51.
[2] C. Soto, S. Pritzkow, Protein misfolding, aggregation, and conformational strains in neurodegenerative diseases, Nature Neurosci. (2018) 1.
[3] M. Jucker, L.C. Walker, Propagation and spread of pathogenic protein assemblies in neurodegenerative diseases, Nature Neurosci. 21 (10) (2018) 1341.
[4] C. Elliott, A.I. Rojo, E. Ribe, M. Broadstock, W. Xia, P. Morin, M. Semenov, G. Baillie, A. Cuadrado, R. Al-Shawi, et al., A role for APP in wnt signalling links synapse loss with β-amyloid production, Transl. Psychiatry 8 (1) (2018) 1–13.
[5] M.M. Pallitto, R.M. Murphy, A mathematical model of the kinetics of β-amyloid fibril growth from the denatured state, Biophys. J. 81 (3) (2001) 1805–1822.
[6] D.L. Craft, L.M. Wein, D.J. Selkoe, A mathematical model of the impact of novel treatments on the aβburden in the Alzheimer's brain, CSF and plasma, Bull. Math. Biol. 64 (5) (2002) 1011–1031.
[7] L. Edelstein-Keshet, A. Spiros, Exploring the formation of Alzheimer's disease senile plaques in silico, J. Theoret. Biol. 216 (3) (2002) 301–326.
[8] B. Franchi, M.C. Tesi, A qualitative model for aggregation-fragmentation and diffusion of β-amyloid in Alzheimer's disease, Rend. Semin. Mat. Univ. Politec. Torino 70 (2012) 75–84.
[9] M. Helal, E. Hingant, L. Pujo-Menjouet, G.F. Webb, Alzheimer's disease: analysis of a mathematical model incorporating the role of prions, J. Math. Biol. 69 (5) (2014) 1207–1235.
[10] B. Franchi, S. Lorenzani, From a microscopic to a macroscopic model for Alzheimer disease: two-scale homogenization of the Smoluchowski equation in perforated domains, J. Nonlinear Sci. 26 (3) (2016) 717–753.
[11] M. Bertsch, B. Franchi, M.C. Tesi, A. Tosin, Microscopic and macroscopic models for the onset and progression of Alzheimer's disease, J. Phys. A 50 (41) (2017) 414003.
[12] L. Desvillettes, S. Lorenzani, Homogenization of the discrete diffusive coagulation–fragmentation equations in perforated domains, J. Math. Anal. Appl. 467 (2) (2018) 1100–1128.
[13] F. Matthäus, The spread of prion diseases in the brain—models of reaction and transport on networks, J. Biol. Systems 17 (04) (2009) 623–641.
[14] Y. Iturria-Medina, R.C. Sotero, P.J. Toussaint, A.C. Evans, et al., Epidemic spreading model to characterize misfolded proteins propagation in aging and associated neurodegenerative disorders, PLoS Comput. Biol. 10 (11) (2014) e1003956.
[15] J. Weickenmeier, E. Kuhl, A. Goriely, Multiphysics of prionlike diseases: Progression and atrophy, Phys. Rev. Lett. 121 (15) (2018) 158101.
[16] J. Weickenmeier, M. Jucker, A. Goriely, E. Kuhl, A physics-based model explains the prion-like features of neurodegeneration in Alzheimer's disease, Parkinson's disease, and amyotrophic lateral sclerosis, J. Mech. Phys. Solids 124 (2019) 264–281.
[17] S. Fornari, A. Schäfer, M. Jucker, A. Goriely, E. Kuhl, Prion-like spreading of Alzheimer's disease within the brain's connectome, J. R. Soc. Interface 16 (159) (2019) 20190356.
[18] S. Fornari, A. Schäfer, E. Kuhl, A. Goriely, Spatially-extended nucleation-aggregation-fragmentation models for the dynamics of prion-like neurodegenerative protein-spreading in the brain and its connectome, J. Theoret. Biol. 486 (2020) 110102.
[19] M. Bertsch, B. Franchi, N. Marcello, M.C. Tesi, A. Tosin, Alzheimer's disease: a mathematical model for onset and progression, Math. Med. Biol. A J. IMA 34 (2) (2017) 193–214.
[20] A. Goriely, E. Kuhl, C. Bick, Neuronal oscillations on evolving networks: Dynamics, damage, degradation, decline, dementia, and death, Phys. Rev. Lett. 125 (12) (2020) 128102.
[21] M. Doi, A. Onuki, Dynamic coupling between stress and composition in polymer solutions and blends, J. Phys. II 2 (8) (1992) 1631–1656.
[22] S.M. Wise, J.S. Lowengrub, H.B. Frieboes, V. Cristini, Three-dimensional multispecies nonlinear tumor growth—I: model and numerical method, J. Theoret. Biol. 253 (3) (2008) 524–543.
[23] H. Byrne, L. Preziosi, Modelling solid tumour growth using the theory of mixtures, Math. Med. Biol. A J. IMA 20 (4) (2003) 341–366.
[24] M. Doi, Soft Matter Physics, Oxford University Press, 2013.
[25] C. Chatelain, T. Balois, P. Ciarletta, M.B. Amar, Emergence of microstructural patterns in skin cancer: a phase separation analysis in a binary mixture, New J. Phys. 13 (11) (2011) 115013.
[26] F. Carbonell, Y. Iturria-Medina, A.C. Evans, Mathematical modeling of protein misfolding mechanisms in neurological diseases: a historical overview, Front. Neurol. 9 (2018) 37.
[27] G. D'Arrigo, M. Gabrielli, F. Scaroni, P. Swuec, L. Amin, A. Pegoraro, E. Adinolfi, F. Di Virgilio, D. Cojoc, G. Legname, et al., Astrocytes-derived extracellular vesicles in motion at the neuron surface: Involvement of the prion protein, J. Extracell. Vesicles 10 (9) (2021) e12114.
[28] J.P. Keener, J. Sneyd, Mathematical Physiology 1: cellular Physiology, Springer New York, NY, USA, 2009.
[29] F. Hecht, New development in FreeFem++, J. Numer. Math. 20 (3–4) (2012) 251–265, URL https://freefem.org/.
[30] J. Barrett, J. Blowey, Finite element approximation of the Cahn-Hilliard equation with concentration dependent mobility, Math. Comput. Am. Math. Soc. 68 (226) (1999) 487–517.
[31] A. Agosti, P.F. Antonietti, P. Ciarletta, M. Grasselli, M. Verani, A Cahn-Hilliard–type equation with application to tumor growth dynamics, Math. Methods Appl. Sci. 40 (18) (2017) 7598–7626.
[32] J.W. Barrett, J.F. Blowey, H. Garcke, Finite element approximation of the Cahn–Hilliard equation with degenerate mobility, SIAM J. Numer. Anal. 37 (1) (1999) 286–318.
[33] C.T. Kelley, Iterative Methods for Optimization, SIAM, 1999.
[34] V. Acary, B. Brogliato, Numerical Methods for Nonsmooth Dynamical Systems: Applications in Mechanics and Electronics, Springer Science & Business Media, 2008.
[35] A. Agosti, C. Cattaneo, C. Giverso, D. Ambrosi, P. Ciarletta, A computational framework for the personalized clinical treatment of glioblastoma multiforme, ZAMM-J. Appl. Math. Mech. Z. Angew. Math. Mech. 98 (12) (2018) 2307–2327.
[36] A. Agosti, C. Giverso, E. Faggiano, A. Stamm, P. Ciarletta, A personalized mathematical tool for neuro-oncology: A clinical case study, Int. J. Non-Linear Mech. 107 (2018) 170–181.
[37] C.R. Jack Jr., D.S. Knopman, W.J. Jagust, R.C. Petersen, M.W. Weiner, P.S. Aisen, L.M. Shaw, P. Vemuri, H.J. Wiste, S.D. Weigand, et al., Tracking pathophysiological processes in alzheimer's disease: an updated hypothetical model of dynamic biomarkers, Lancet Neurol. 12 (2) (2013) 207–216.
[38] L. Mosconi, V. Berti, L. Glodzik, A. Pupi, S. De Santi, M.J. de Leon, Pre-clinical detection of alzheimer's disease using FDG-pet, with or without amyloid imaging, J. Alzheimer's Dis. 20 (3) (2010) 843–854.
[39] M. Bertsch, B. Franchi, A. Raj, M.C. Tesi, Macroscopic modelling of Alzheimer's disease: difficulties and challenges, Brain Multiphys. 2 (2021) 100040.